Scalable Formation of Carbon Nanotube Films Containing Highly Aligned Whiskerlike Crystallites

Anson W. K. Ma,[†,‡,§] Jaewook Nam,[†,‡,○] Natnael Behabtu,[†,‡] Francesca Mirri,[†,‡] Colin C. Young,[†,‡] Budhadipta Dan,[†,‡] Dmitri Tsentalovich,[†,‡] Mainak Majumder,[†,‡] Li Song,[‡,⊥] Yachin Cohen,[△] Pulickel M. Ajayan,[†,‡,‖] and Matteo Pasquali*[,†,‡,‖]

[†]Department of Chemical and Biomolecular Engineering, [‡]The Smalley Institute for Nanoscale Science and Technology, [⊥]Department of Mechanical Engineering & Materials Science, and [‖]Department of Chemistry, Rice University, 6100 Main Street, Houston, Texas 77005, United States

[§]Department of Chemical and Biomolecular Engineering & Institute of Materials Science, University of Connecticut, 97 N. Eagleville Road, Storrs, Connecticut 06103, United States

[○]School of Chemical Engineering, Sungkyunkwan University, Suwon 440-746, Korea

[△]Department of Chemical Engineering, Technion—Israel Institute of Technology, Haifa 32000, Israel

ABSTRACT: We report the creation of carbon nanotube films from superacids by a scalable process, where film morphology is controlled by initial fluid phases. These films were formed by dip-coating biphasic (isotropic + liquid crystalline) carbon nanotube (CNT) chlorosulfonic acid solutions. Chlorosulfonic acid has low volatility and is therefore removed by solvent extraction instead of conventional drying processes. At intermediate concentrations, the solutions contain liquid crystalline domains which stretch and align streamwise during dip-coating. These elongated domains further act as "nucleating sites" for large, aligned whiskerlike crystallites during subsequent solvent extraction. The final films contain highly aligned CNT crystallites embedded in a mesh of randomly oriented CNTs.

Because of their fascinating properties, carbon nanotubes (CNTs) have been studied intensely for the past two decades.[1−5] Realizing these properties in macroscopic functional materials requires the ability to manipulate and control CNT assemblies across multiple length scales.[6−8] CNTs can be processed into neat[9−12] or composite[13,14] fibers, while CNT films can be produced from solutions of surfactant stabilized or functionalized CNTs by filtration,[13−21] inkjet printing,[22−24] spray coating,[25] rod coating,[26] drop casting,[27] and dip-coating.[28,29] Surfactant-stabilized CNT dispersions must be sonicated, which is known to shorten CNTs;[30−32] any residue surfactant in the films increases the electrical resistivity.[26] Covalent functionalization damages the conjugated sp^2 bonds and hence destroys the electrical properties of CNTs. Film-forming methods produce films of isotropically orientated CNTs, with only a few exceptions. Pint et al.[33] detached vertically aligned CNT arrays from the catalyst and "dry printed" the arrays onto any surface by using the substrate as the stamp. In wet processes, strong magnetic fields were used to align the CNTs during the filtration of CNT−surfactant solutions,[13,16,34,35] creating films with anisotropic transport properties. Windle et al. showed that, when dispersed at high concentration, oxidized multiwalled CNTs formed liquid crystalline structures with local CNT orientational ordering.[36−38] Inspired by this finding, Zhou and co-workers[28,29] prepared aqueous solutions of oxidized CNTs and gradually evaporated the water solvent as a glass substrate was placed into the CNT solution. As the water evaporated the local CNT concentration increased, yielding the formation of ordered CNT structures along the triple line—the interface between air, liquid, and the solid substrate.

These structures were then deposited onto a stationary or moving substrate and were used as a template for liquid crystal displays.[28] In the case of CNT fibers, a high degree of alignment was obtained from fluid phase processing, namely by spinning from liquid crystalline solutions of CNTs in superacids.[11,39] Film formation from acid solutions was demonstrated by filtration (in the case of dilute solutions)[40,41] and by spreading high-concentration dopes.[39] More recently, dip-coating has been used to produce isotropic, homogeneous thin films from CNT−superacid solutions.[42,43]

Here, we present a scalable method to produce a novel type of CNT film containing highly aligned, whiskerlike CNT crystallites, which may reinforce the thin films. This novel structure is obtained by combining self-assembly (liquid crystal formation of CNTs in superacids), flow-directed assembly, and rapid solvent extraction with a low-viscosity fluid. The CNT thin films can potentially be used as filter membranes[44−46] and transparent, conductive, and flexible coatings for touch screens and organic light-emitting diode applications.[26,41,43,47−49] With further process refinement and postprocessing, these films could be engineered to display anisotropic mechanical and electrical properties.
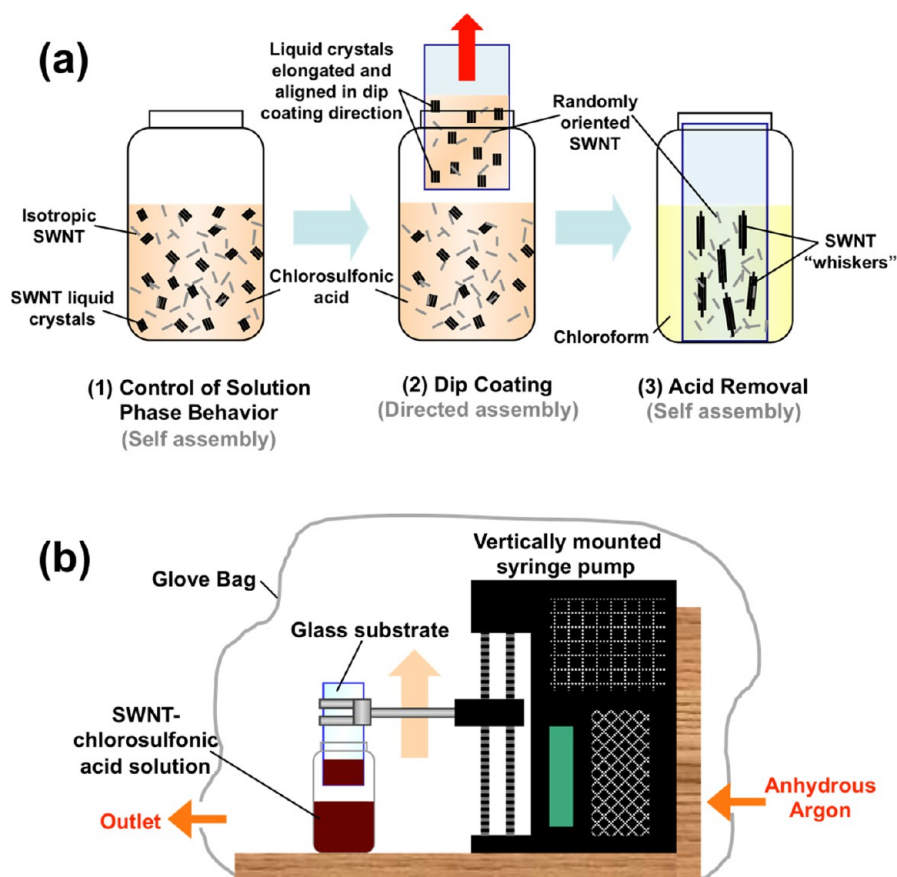
Figure 1. (a) Schematic illustration of the film formation process consisting of three main steps. (1) Self-assembly: SWNTs are dissolved in chlorosulfonic acid creating a biphasic solution which contains SWNT liquid crystals and individually dispersed (isotropic) SWNTs. (2) Directed assembly: dip-coating is then applied to produce a wet film containing elongated and aligned liquid crystals. (3) Self-assembly: by removing the acid solvent, the prealigned liquid crystals serve as the nucleating sites for whiskerlike crystallites. (b) Experimental setup for dip-coating the SWNT-chlorosulfonic acid solutions. Both the dip-coating and acid removal steps were carried out inside a glovebag constantly purged with anhydrous argon to avoid moisture contamination.

■ RESULTS AND DISCUSSION

Formation of Whiskerlike SWNT Crystallites from Biphasic Solutions. Single-walled CNT (SWNT) films were formed in a three-step process: (1) formation of a superacid solution, (2) coating the solution on a glass substrate, and (3) consolidation of structure through solvent removal by immersion in chloroform (Figure 1). Solution concentration plays a fundamental role in controlling the film morphology. Low concentration solutions of CNTs in superacids form isotropic phases (the CNTs are randomly oriented in the solution). As the CNT concentration increases, excluded volume interactions cause the formation of liquid crystalline (LC) domains consisting of aligned CNTs, which coexist with the isotropic phase.[39,50−52] In this biphasic regime, concentration and acid strength control the morphology of the LC domains, which can vary from nearly endless threads (spaghetti) to ellipsoidal tactoids as the solvent goes from sulfuric to chlorosulfonic acid.[39,50,53] At even higher concentrations, CNTs in acids form a LC with polydomain morphology. To attain films containing highly aligned, whisker-like SWNT crystallites, dubbed hereafter "SWNT whiskers", biphasic CNT solutions were used. Figure 2 shows transmitted light micrographs of films obtained at different solution concentrations (from 0.5 to 1 vol %). All the films show preferential orientation in the dip-coating direction due to the LC alignment during substrate withdrawal. Optical and electron microscopy

showed no noticeable change in whisker dimensions as the concentration and coating rate were varied between 0.5% to 1% and between 0.3 and 3 mm/s, respectively. In the case of isotropic solutions (0.1% and 0.2 vol %), thin films with a thickness of less than 30 nm were produced, but these films showed no optical birefringence and consisted of randomly oriented SWNTs (Figure 2a−c). The films dip-coated from the 0.1% and 0.2% solutions have an average transmittance of 90% and 67% (at 550 nm), and an average sheet resistance of 1530 and 135 Ω/sq, respectively, potentially useful as flexible, transparent, and conductive coatings for touch screen applications.[41,43]

Figure 3 shows the optical microstructure of a biphasic solution—0.7 vol % SWNT in chlorosulfonic acid—captured using transmitted light, with (Figure 3b) and without (Figure 3a) cross-polarizers. As shown in the polarized light micrograph (Figure 3b), several discrete LC structures in the solution show optical birefringence ("lit up"), indicating intrinsic alignment of SWNT within these structures. These LC structures have a peculiar ellipsoidal shape (tactoid), likely due to the strong elastic energy (splay and bend) and low interfacial tension in the system. Similar tactoid LC structures were recently observed in aqueous dispersions of bile-salt stabilized SWNTs.[54] Unlike the convective assembly method reported for aqueous CNT solutions,[26,27] where the gradual evaporation needed to concentrate the solution and form a liquid crystal occurs over several days, the acid removal process is much faster (minutes or less).
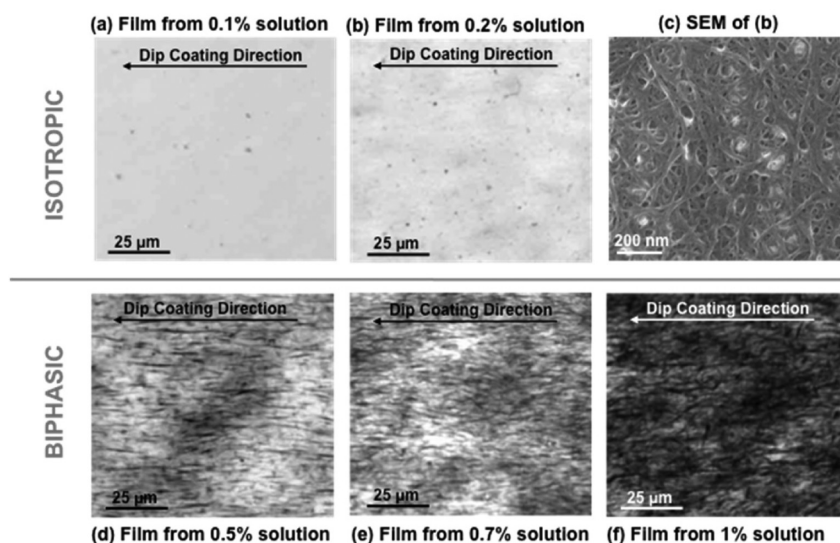
Figure 2. Transmitted light micrographs of dried films dip-coated from isotropic solutions: (a) 0.1% and (b) 0.2% SWNT in chlorosulfonic acid. (c) Scanning electron microscopy (SEM) image of film shown in part b. (d−f) Transmitted light micrographs of dried films dip-coated from biphasic solutions: (d) 0.5%, (e) 0.7%, and (f) 1%, respectively.
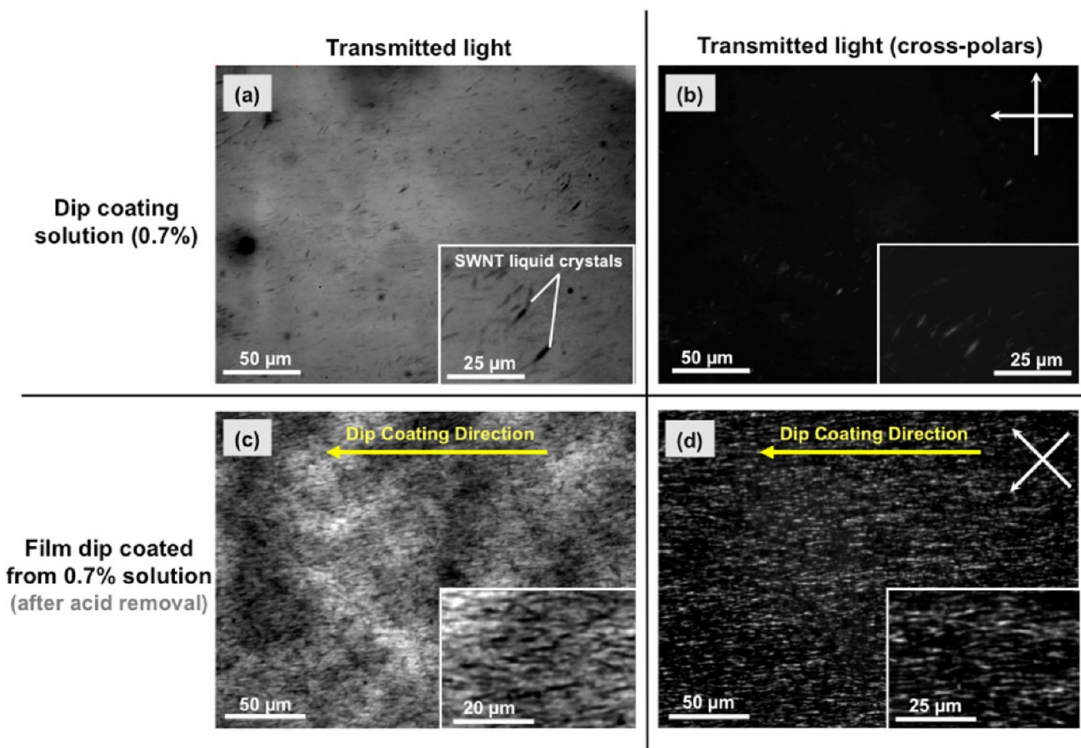
Figure 3. (a and b): Optical micrographs of the dip-coating solution containing 0.7 vol % SWNT in chlorosulfonic acid, imaged using (a) transmitted light and (b) transmitted light with cross-polarizers. The solution sample was sealed between a glass microscope slide and a coverslip using aluminum tape. (c and d) Optical micrographs of the corresponding dip-coated films (after acid removal) imaged under (c) transmitted light and (d) transmitted light with cross-polarizers. The dip-coating direction was horizontal as indicated.

Figures 3c and d show representative light micrographs of the resulting film captured using transmitted light (with and without cross-polarizers). The resulting film contains structures that are preferentially aligned along the dip-coating direction. No preferential alignment of LC domains is observed in the biphasic solutions; therefore, the streamwise alignment must be caused by the dip-coating process. Because the LC domains are fluid, they may undergo stretching in addition to alignment in the high shear film formation zone. These elongated LC domains then act as nucleating sites for the further growth of large, SWNT whiskers during the subsequent acid removal process (Figure 1). SWNT whiskers are typically 10−20 μm long and ∼100 nm thick. They are strongly birefringent in polarized light microscopy (Figure 3d), indicating that the SWNTs within these structures are highly aligned. It is worth noting that in the case of thermotropic liquid crystalline polymers, macroscopic alignment
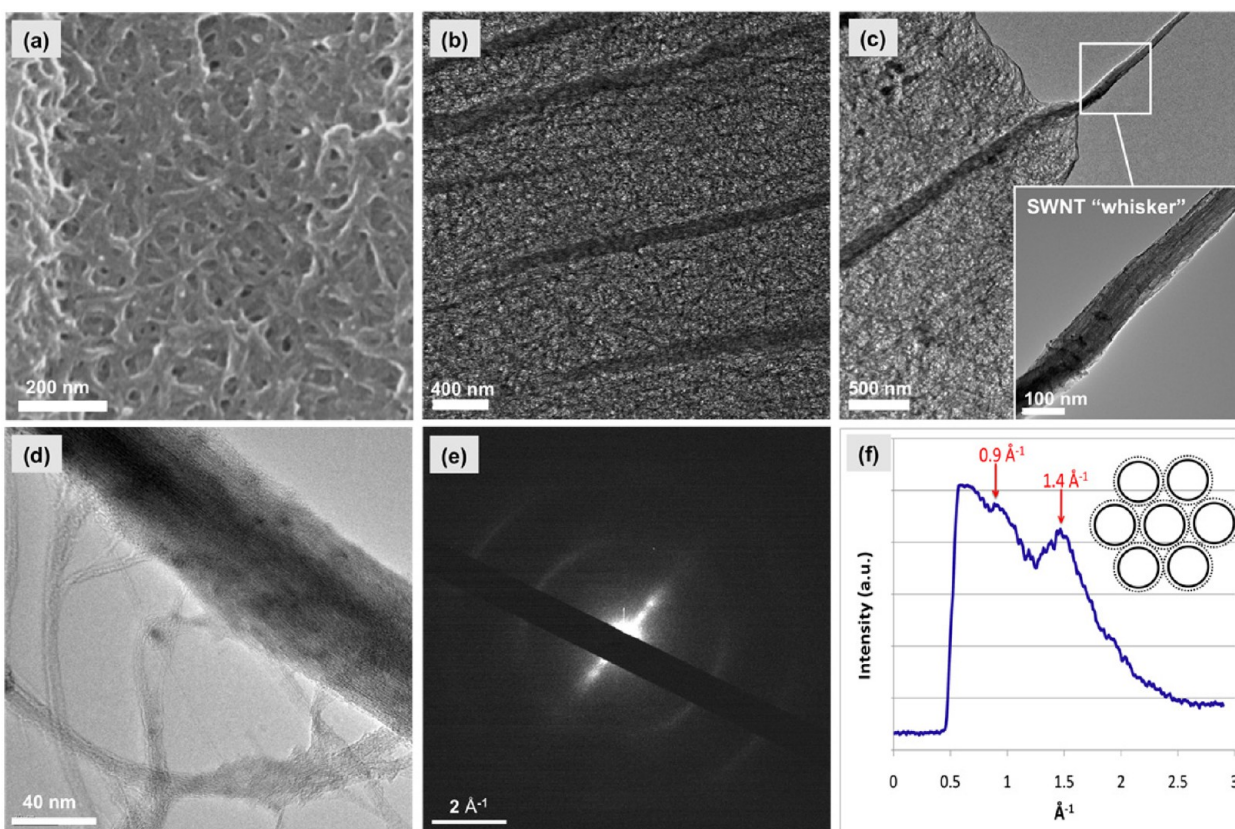
Figure 4. (a) SEM image and (b) transmission electron microscopy (TEM) image of a dried SWNT film produced from the 0.5 vol % SWNT-chlorosulfonic acid solution. (c) SWNT whisker with a diameter of ∼100 nm protruding out of a random SWNT network. (d) High magnification image of an *SWNT whisker* showing a high degree of SWNT alignment. The electron diffraction pattern of the same whisker is shown in e. (f) Central line profile of an SWNT whisker, indicating triangular lattice packing.

of polymer crystallites can be obtained by applying shear to the specimen during annealing.[55,56] In this paper, we show that by using the right solvent and processing flow conditions, SWNTs can be processed in a similar way to obtain crystallite structures with macroscopic alignment.

Transmission and scanning electron microscopy (TEM and SEM) were performed on the dried films. Interestingly, SWNT whiskers are only visible in transmission mode (TEM) (Figures 4b and c) but not in surface scanning mode (SEM) (Figure 4a), indicating that these structures are embedded within a random network of SWNTs. This is similar to the case of crystallites found in polymer melt systems, where crystallites cannot be captured by SEM unless the amorphous portion of the specimen is etched selectively.[55,57−59] TEM shows that SWNT whiskers typically have a maximum width of 100 nm; their alignment cannot be resolved from Figure 4b because the whiskers are embedded in a random SWNT network. When part of the film was broken and transferred from the glass substrate onto a TEM grid (see Methods), some SWNT whiskers protruded out of the random network at the edge of the specimen (Figure 4c). Clear alignment of SWNT within the whisker is shown in Figure 4d; Figure 4e shows the corresponding electron diffraction pattern containing information about SWNTs packing within the whisker. Henrard et al.[60] showed in their electron diffraction simulations and experiments that clear peaks along the central line are present in SWNT bundles, due to the tubes being packed in a triangular lattice. The exact position and breadth of these peaks are influenced by average diameter, diameter distribution, and overall alignment.[61,62] Although we did not attempt a

quantitative fitting, we observed two peaks at 0.9 and 1.4 Å^{-1} along the central line of the electron diffraction of the SWNT whisker (Figure 4f), in qualitative accord with the published patterns.[60] This indicates that SWNTs are aligned and packed in a crystalline manner (inset of Figure 4f). The first and second layer lines are neither uniformly intense, nor clearly spotty. Such features indicate that the SWNT whiskers are made of SWNTs with mixed chirality.

Macroscopic Alignment of "SWNT Whiskers". To understand the alignment of SWNT whiskers, two-dimensional steady state flow equations were solved numerically by using a previously published Galerkin-finite element method (G/FEM).[63,64] Specifically, at the continuum level, the fluid flow is described by the momentum and continuity equations:

$$\rho\mathbf{u}\cdot\nabla\mathbf{u} = \nabla\cdot\mathbf{T} + \rho\mathbf{g} \tag{1}$$

$$\nabla\cdot\mathbf{u} = 0 \tag{2}$$

where $\mathbf{T} = -p\mathbf{I} + \eta(\dot{\gamma}_s)(\nabla\mathbf{u} + (\nabla\mathbf{u})^T)$. For. For a power-law fluid, the generalized Newtonian viscosity is defined as $\eta(\dot{\gamma}_s) = K\dot{\gamma}_s^{n-1}$. Here, we use a scalar shear rate $\dot{\gamma}_s = 2(\mathrm{IIs})^{1/2}$, where IIs is a second invariant of strain rate tensor $\mathbf{S} = 1/2(\nabla\mathbf{u} + (\nabla\mathbf{u})^T)$. In a dip-coating model, the shape and location of the free surface are unknown a priori and are computed as part of the solution. This was done by mapping unknown physical domain onto a known, convenient computational domain by means of elliptic equations. Figure 5 shows the geometry parameters and the boundary conditions used in the two-dimensional model. For steady-state flows, the liquid loss through the outflow boundary needs to be compensated by flow through an artificial inlet.
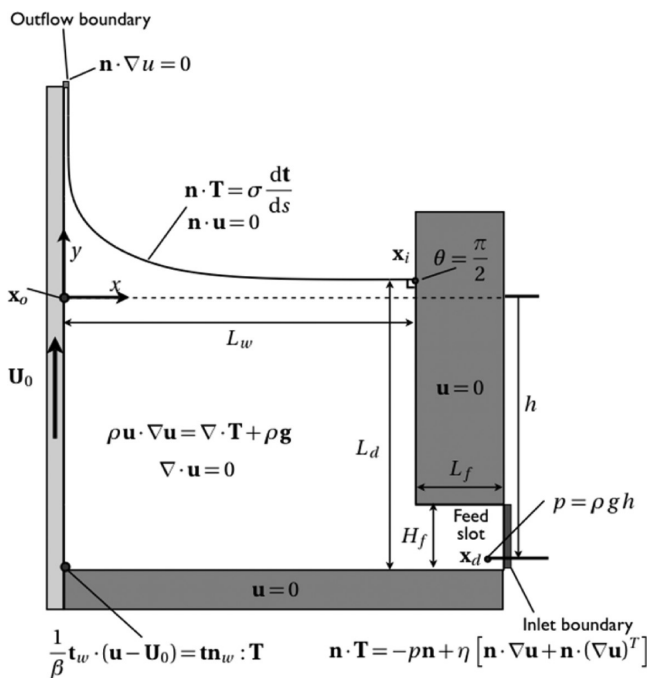
Figure 5. Geometry parameters and boundary conditions for the computational dip-coating model.

We imposed the free boundary condition at the inlet plane.[65] The size of the liquid pool was controlled by the pool width L_w and the pool depth L_d. The pool width needs to be long enough to have vanishing free surface curvature; the minimum acceptable width was computed by direct tracking of the flow feature.[64] For example, the minimum width for $C_{SWNT} = 0.5\%$ is 7.99 mm. Therefore, we fixed $L_w = 8$ mm for all computations. Likewise, L_d

was chosen to be 6 mm. The liquid level was set by pressure inside the liquid pool. In order to maintain the level close to $y = 0$, we imposed the hydrostatic pressure ($P = \rho g h$) at the bottom of the pool.

Figure 6d shows a streamline plot. Only a small portion of liquid from the liquid pool is entrained to form the thin liquid layer; most of the liquid is rejected to the liquid pool. The shear rate inside the liquid entrainment area (shaded region in Figure 6d) was used to estimate the average shear rate ($\bar{\dot{\gamma}}_s$) and residence time (t_R). The input parameters for the modeling were obtained by fitting the rheological data to a power-law fluid model (Figure 7a). The surface tension of the chlorosulfonic acid solutions was measured to be 22.31 mN/m using the pendant drop method (KSV CAM 200 Contact Angle Tool). Figure 6a–c shows the shear rate profile generated during the dip-coating process for different concentrations of SWNT solutions. In the dip-coating process, the highest local shear rate $\dot{\gamma}_{s,max}$ occurs close to the moving substrate and decreases to zero as the free surface is approached. The average shear rate is defined as

$$\bar{\dot{\gamma}}_s = \frac{\int_{A_e} \dot{\gamma}_s \, dA}{\int_{A_e} dA} = \frac{\int_{A_e} \dot{\gamma}_s \, dA}{A_e} \tag{3}$$

where A_e is the liquid entrainment area, and it contains elements with a stream function value higher than that at the separating streamline (Figure 6d). For SWNTs and LC structures to align, the Péclet number should be large, i.e., $Pe = (\dot{\gamma}_s/D_r) \gg 1$. If we assume the LC structures are discrete spheroids embedded in a matrix of individually dispersed SWNTs, the rotary diffusivity can be estimated using the following equation:[66]

$$D_r = \frac{3k_B T(\ln(2p - 0.5)}{\pi \eta L^3} \tag{4}$$
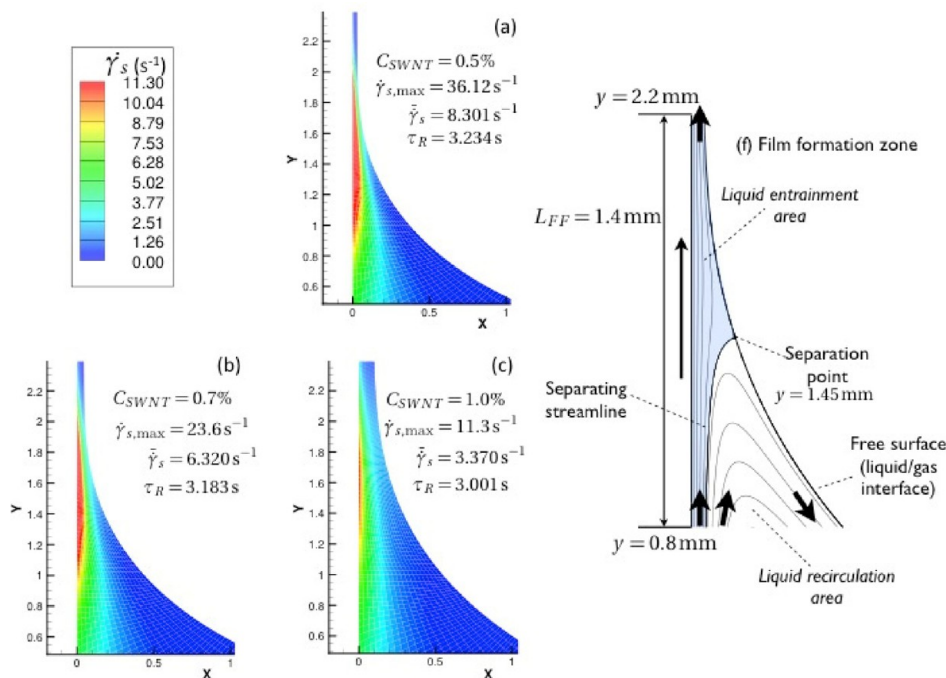
Figure 6. Shear rate profile for different concentrations of dip-coating solutions calculated from the 2D flow analysis: (a) 0.5, (b) 0.7, and (c) 1 vol % SWNT in chlorosulfonic acid. The dip-coating solutions are assumed as a power-law fluid (Figure 7a). The values of maximum shear rate (close to the glass substrate), average shear rate, and residence time are given for each dip-coating solution. (d) Streamline plot showing the liquid entrainment area (A_e).
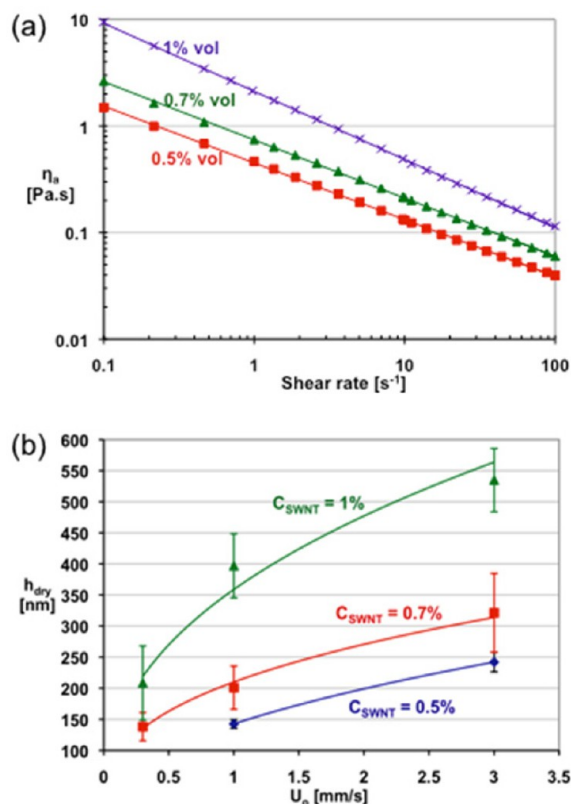
Figure 7. (a) Steady shear rheology of different concentrations (vol %) of dip-coating solutions characterized using a stress-controlled rheometer (AR 2000ex; TA Instruments) enclosed inside a custom-made glovebox constantly purged with dry air. Relative humidity during sample loading and testing was kept below 2–3%. Parallel plate geometry made of stainless steel (SS 316) was used. Lines are data fitting to a power law fluid model. η_a is the apparent shear viscosity. (b) Dry film thickness (h_{dry}) of films dip-coated at different substrate withdrawal speeds for three different concentrations (C_{SWNT}) of SWNT in chlorosulfonic acid. The lines are power-law fits. The error bar of each data point represents the standard deviation of nine measurements (three films dip-coated from the same solution and three measurements are carried out at various locations on each film). The film sheet resistance values corresponding to 0.5, 0.7, 1 vol % concentrations are 62 ± 35, 22 ± 1, and 8 ± 3 Ω/sq, respectively.

where k_B is the Boltzmann constant, T is temperature, L is the length of LC structures ($\sim 4 \, \mu$m), and p is the ratio of the length to the width of LC structures (~ 4). η was measured to be ~ 100 mPa s at a shear rate of 40 s^{-1}. This gives a rotary diffusivity of ~ 0.001 s^{-1} for the LC structures. The highest local shear rate $\dot{\gamma}_{s,max}$ generated from dip-coating biphasic solutions ranges from 11–36 s^{-1}. Therefore, the Pe number for LC structures is of the order of 10 000 (indicating strong flow alignment). Further, the rotational relaxation time $\tau_r = 1/6D_r$ of the whiskers is in the range of tens of minutes, indicating that the whiskers cannot reorient before solvent extraction. Conversely, the isotropic phase contains individual SWNTs with an estimated rotational relaxation time on the order of less than a second.[67,68] The corresponding Pe number is 2–3 orders of magnitude smaller than that of the whiskers. Although long individual SWNTs may align during flow in the meniscus region, the residence time in the flat film and the subsequent transfer time into the chloroform bath are sufficiently long for randomization of the alignment of any aligned individual SWNTs. This may explain the presence of an isotropic SWNT network in the final films.

Discrete LC structures deform when the hydrodynamic forces are strong enough to overcome the elastic and interfacial ones. The capillary number Ca is defined as

$$Ca = \frac{\eta \dot{\gamma} d}{\sigma} \tag{5}$$

where η is ~ 100 mPa s, $\dot{\gamma} = \dot{\gamma}_{s,max} = \sim 40$ s^{-1}, and d is the width of LC structures ($\sim 1 \, \mu$m). For an LC structure suspended within an "isotropic SWNT" medium, Ca is estimated to be ~ 4, implying that the flow-induced shear stresses exceed the interfacial tension of the LC tactoids. The *Ericksen* number is the ratio of viscous to elastic stresses:

$$Er = \frac{\eta \dot{\gamma}}{K/L^2} \tag{6}$$

K is estimated to be $\sim 5 \times 10^{-12}$ N by assuming a surface tension σ on the order of μN/m and a value of $K/\sigma = \sim 5 \, \mu$m.[54] The exact K value for superacid systems may be different than the assumed value, and the K value is assumed for an order-of-magnitude scaling analysis. Er is estimated to be ~ 13, which implies the shear stresses are sufficiently high to overcome the elastic stresses, leading to deformation of the domains. This simple scaling analysis suggests that the discrete LC structures are stretched in the high shear flow during film formation. Equation 4 is useful for estimating whether the hydrodynamics forces were sufficiently large to align the whiskers during dip-coating. However, the equation also assumes the whiskers behave as rigid entities and the rotary diffusivity is well-defined. To examine this assumption, a simple scaling analysis (eqs 5 and 6) was performed to compare the hydrodynamic forces with the elastic and interfacial forces. The results suggested that the hydrodynamic forces experienced by the whiskers are sufficiently large to deform the whiskers. For the flow conditions considered, it is more appropriate to treat whiskers as deformable objects.

The orientation distribution of whiskers and the angle of misalignment from the dip-coating direction were calculated using ImageJ with plugin "OrientationJ".[69] As shown in Table 1,

Table 1. Degree of Whisker Misalignment ($\langle \theta^2 \rangle^{1/2}$) for Films Dip-Coated from Different Concentrations of SWNT−Acid Solutions (0.5%, 0.7%, and 1%)[a]

films dip-coated from	$\langle \theta^2 \rangle^{1/2}$
0.5%	$\pm 10.4°$
0.7%	$\pm 10.4°$
1%	$\pm 14.1°$

[a]Where θ is the angle between the whisker axis and the dip-coating direction. The orientation distribution of whiskers was calculated from the optical micrographs using ImageJ plugin OrientationJ, and each reported $\langle \theta^2 \rangle^{1/2}$ value was averaged over three arbitrarily chosen areas (300 μm $\times$ 300 μm).

whiskers in 1% film have a larger angle of misalignment ($\pm 14.1°$) from the dip-coating direction compared with those in the 0.5% and 0.7% films ($\pm 10.4°$). This can be explained by considering the shear rate and strain experienced by LC structures. As the solution concentration increases, both the maximum $\dot{\gamma}_{s,max}$ and average shear rate $\dot{\gamma}_s$ decrease. The residence time t_R is

$$t_R = \frac{\int_{A_e} dA}{q} = \frac{A_e}{q} \tag{7}$$

where q is the flow rate (2D) through the outflow boundary. Because the flow rate q grows faster than the liquid entrainment area A_e, both the residence time t_R and the total strain ($= \bar{\dot{\gamma}}_s \cdot t_R$) experienced by the SWNT decrease. The lower alignment in the 1% film can therefore be explained by (1) lower (average) shear rate and (2) smaller strain experienced by the LC structures during the dip-coating process.

Film Thickness and Sheet Resistance. Film thickness depends on SWNT concentration and substrate withdrawal speed. For a fixed substrate withdrawal speed, lower concentration solutions produce thinner films because they have lower viscosities and contain fewer SWNTs. Figure 7b shows film thickness (after acid removal) as a function of substrate withdrawal speed. Gutfinger and Tallmadge[70] applied lubrication analysis to power-law fluids ($\eta_a = K\dot{\gamma}^{n-1}$) and showed that the film thickness should scale as $h_{dry} \propto h_{wet} \propto U_o^{[2n/(2n+1)]}$, where U_o is the substrate withdrawal speed. Table 2 compares the predicted

Table 2. Scaling Exponent (α) for Film Thickness (h) as a Function of Substrate Withdrawal Speed (U_o; i.e., $h_{dry} \propto U_o^{\alpha}$)[a]

C_{SWNT}	n value from rheology	α predicted in lubrication analysis (i.e., $2n/(2n+1)$)	α from Figure 7b
0.5%	0.47	0.49	0.48
0.7%	0.45	0.48	0.37
1.0%	0.36	0.42	0.41

[a]Comparison between α obtained from lubrication analysis[70] and from Figure 7b.

scaling exponents (using n values from rheological measurements) with those determined from Figure 7b. The values for 0.5% solution agree to within ~2% and those for the 0.7% solution agree to within ~20%.

Films dip-coated from higher concentrations of SWNT are thicker and have lower sheet resistance. On the basis of the sheet resistance and thickness data, the conductivity for the 0.5%, 0.7%, and 1% films varies from 1.1×10^5 S/m to 3.1×10^5 S/m (sheet resistance from 62 ± 35 to 8 ± 3 Ω/sq), which is comparable to values reported for SWNT films produced from filtration[35,41] (using HiPco SWNT) and acid doped SWNT fibers[11] (5×10^5 S/m). Conductivity of the films was measured both along and perpendicular to the dip-coating direction, and the results showed no dependence on the direction of measurements. For future work, it is of interest to measure the mechanical properties of the films to examine: (i) if the CNT crystallites mechanically reinforce the thin film and (ii) if the films display any anisotropic mechanical properties. Although most of the acid was removed during the coagulation step, the films were naturally doped with trace amounts of adsorbed acid, which increased their conductivity.[25,26,71] Acid doping was removed by heat treatment, yielding ~3-fold higher sheet resistance after heating at 150 °C for 24 h.

CONCLUSIONS

In summary, we have presented the formation of whiskerlike crystallite structures from biphasic solutions of CNTs in superacids. These whiskerlike structures consist of SWNTs that are highly aligned and closely packed in a crystalline manner. They have a maximum width of ~100 nm and a typical length of 10−20 μm. Interestingly, the whiskers are macroscopically aligned in the dip-coating direction and are interspersed within an isotropic SWNT network. Presumably, the alignment of SWNT within the whiskers results from the pre-existing liquid

crystalline alignment, while the alignment of the LC structures was caused by the coating flow. Further, the shear forces generated during the dip-coating were sufficiently high enough to overcome the elastic and interfacial forces, leading to elongated LC structures. Notably, the film-formation method closely resembles the processing of liquid crystalline polymers into films with aligned crystalline structures, confirming further that, with the right solvent, polymer processing techniques can be readily adapted to CNT material processing.[39,72,73]

METHODS

Materials and SWNT Solution Preparation. Carbon nanotubes used in this study are single-walled nanotubes (SWNTs) produced using the high pressure carbon monoxide (HiPco) method[74] (Rice University; batch no. 188.2). The HiPco SWNTs have an average length of 500 nm[68] and average diameter of ~1 nm. The amorphous carbon and iron catalyst were removed by oxidizing at a temperature of 375 °C in the presence of SF_6 and O_2, followed by washing with 6 M HCl at 90 °C. Dip-coating solutions were prepared by stir-bar mixing for 24 h. A volume fraction was calculated by assuming a density of 1300 kg/m^3 for the SWNTs.

Film Formation Process. The actual dip-coating setup consists of a vertically mounted syringe pump (Harvard Apparatus PHD 2000) as shown in the schematic diagram (Figure 1b). Different withdrawal speeds were obtained by controlling the volumetric flow rates for an arbitrarily assigned syringe diameter. The dip-coated film contained both SWNT and the solvent (i.e., chlorosulfonic acid); as soon as the liquid film was withdrawn from the dip-coating solution, it was immersed in chloroform for at least 15 min to remove the acid as described elsewhere.[43] It should be noted that upon moisture exposure, chlorosulfonic acid decomposes into hydrochloric gas (HCl) and sulfuric acid (H_2SO_4), causing film breakage due to the fast HCl release. To avoid moisture contamination, the whole operation was carried out inside a glovebag constantly purged with anhydrous argon gas (Figure 1b).

Characterization. Light microscopy images of the dip-coating solutions and final SWNTs films were captured using a Zeiss Axioplan optical microscope. Liquid samples were prepared inside an anhydrous glovebox as described in ref 50, where the sample solution was confined between a microscope slide and coverslip and sealed with aluminum tape. SEM images were captured using JEOL 6500F. For TEM samples, the SWNT film was detached from the glass substrate by submerging the sample into DI water; a TEM grid was then used to recover the detached part of the film for imaging (JEOL 2010, 100 kV). Steady shear rheology of the solutions was characterized using a stress-controlled rheometer (AR 2000ex; TA Instruments) enclosed inside a custom-made glovebox constantly purged with dry air. Relative humidity during sample loading and testing was kept below 2−3%. Parallel plate geometry made of stainless steel (SS 316) was used. SWNT film thickness (after chloroform quenching) was measured using mechanical profilometer (Vecco Dektak 6M). The error bar of each data point in Figure 7b represents the standard deviation of nine measurements (three films were dip-coated from the same solution and three measurements were performed at various locations on each film). Sheet resistance was measured using the 4-point probe method (Jandel).

AUTHOR INFORMATION

Corresponding Author
*E-mail: mp@rice.edu.

■ **REFERENCES**

(1) Iijima, S. Helical Microtubules of Graphitic Carbon. *Nature* **1991**, *354*, 56−58.

(2) Baughman, R. H.; Zakhidov, A. A.; de Heer, W. A. Carbon Nanotubes - the Route toward Applications. *Science* **2002**, *297*, 787−792.

(3) Tomanek, D.; Jorio, A.; Dresselhaus, M. S.; Dresselhaus, G., Introduction to the Important and Exciting Aspects of Carbon-Nanotube Science and Technology. In *Carbon Nanotubes*; Springer-Verlag: Berlin, 2008; Vol. *111*, pp 1−12.

(4) Avouris, P. Molecular Electronics with Carbon Nanotubes. *Acc. Chem. Res.* **2002**, *35*, 1026−1034.

(5) Thostenson, E. T.; Ren, Z. F.; Chou, T. W. Advances in the Science and Technology of Carbon Nanotubes and Their Composites: A Review. *Compos. Sci. Technol.* **2001**, *61*, 1899−1912.

(6) Wang, X.; Zhuang, J.; Peng, Q.; Li, Y. D. A General Strategy for Nanocrystal Synthesis. *Nature* **2005**, *437*, 121−124.

(7) Rao, C. N. R.; Cheetham, A. K. Science and Technology of Nanomaterials: Current Status and Future Prospects. *J. Mater. Chem.* **2001**, *11*, 2887−2894.

(8) Ariga, K.; Hill, J. P.; Lee, M. V.; Vinu, A.; Charvet, R.; Acharya, S. Challenges and Breakthroughs in Recent Research on Self-Assembly. *Sci. Tech. Adv. Mater.* **2008**, 9.

(9) Behabtu, N.; Green, M. J.; Pasquali, M. Carbon Nanotube-Based Neat Fibers. *Nano Today* **2008**, *3*, 24−34.

(10) Li, Y. L.; Kinloch, I. A.; Windle, A. H. Direct Spinning of Carbon Nanotube Fibers from Chemical Vapor Deposition Synthesis. *Science* **2004**, *304*, 276−278.

(11) Ericson, L. M.; Fan, H.; Peng, H. Q.; Davis, V. A.; Zhou, W.; Sulpizio, J.; Wang, Y. H.; Booker, R.; Vavro, J.; Guthy, C.; et al. Macroscopic, Neat, Single-Walled Carbon Nanotube Fibers. *Science* **2004**, *305*, 1447−1450.

(12) Zhang, M.; Atkinson, K. R.; Baughman, R. H. Multifunctional Carbon Nanotube Yarns by Downsizing an Ancient Technology. *Science* **2004**, *306*, 1358−1361.

(13) Fischer, J. E.; Zhou, W.; Vavro, J.; Llaguno, M. C.; Guthy, C.; Haggenmueller, R.; Casavant, M. J.; Walters, D. E.; Smalley, R. E. Magnetically Aligned Single Wall Carbon Nanotube Films: Preferred Orientation and Anisotropic Transport Properties. *J. Appl. Phys.* **2003**, *93*, 2157−2163.

(14) Wu, Z. C.; Chen, Z. H.; Du, X.; Logan, J. M.; Sippel, J.; Nikolou, M.; Kamaras, K.; Reynolds, J. R.; Tanner, D. B.; Hebard, A. F.; et al. Transparent, Conductive Carbon Nanotube Films. *Science* **2004**, *305*, 1273−1276.

(15) Green, A. A.; Hersam, M. C. Colored Semitransparent Conductive Coatings Consisting of Monodisperse Metallic Single-Walled Carbon Nanotubes. *Nano Lett.* **2008**, *8*, 1417−1422.

(16) Casavant, M. J.; Walters, D. A.; Schmidt, J. J.; Smalley, R. E. Neat Macroscopic Membranes of Aligned Carbon Nanotubes. *J. Appl. Phys.* **2003**, *93*, 2153−2156.

(17) Hobbie, E. K.; Simien, D. O.; Fagan, J. A.; Huh, J. Y.; Chung, J. Y.; Hudson, S. D.; Obrzut, J.; Douglas, J. F.; Stafford, C. M. Wrinkling and Strain Softening in Single-Wall Carbon Nanotube Membranes. *Phys. Rev. Lett.* **2010**, *104*, 125505.

(18) Harris, J. M.; Iyer, G. R. S.; Bernhardt, A. K.; Huh, J. Y.; Hudson, S. D.; Fagan, J. A.; Hobbie, E. K. Electronic Durability of Flexible Transparent Films from Type-Specific Single-Wall Carbon Nanotubes. *ACS Nano* **2011**, *6*, 881−887.

(19) Harris, J. M.; Iyer, G. R. S.; Simien, D. O.; Fagan, J. A.; Huh, J. Y.; Chung, J. Y.; Hudson, S. D.; Obrzut, J.; Douglas, J. F.; Stafford, C. M.; et al. Structural Stability of Transparent Conducting Films Assembled from Length Purified Single-Wall Carbon Nanotubes. *J. Phys. Chem. C* **2011**, *115*, 3973−3981.

(20) Hecht, D.; Hu, L. B.; Gruner, G. Conductivity Scaling with Bundle Length and Diameter in Single Walled Carbon Nanotube Networks. *Appl. Phys. Lett.* **2006**, *89*, 133112−133111−133113.

(21) Hu, L.; Hecht, D. S.; Grüner, G. Percolation in Transparent and Conducting Carbon Nanotube Networks. *Nano Lett.* **2004**, *4*, 2513−2517.

(22) Shigematsu, S.; Ishida, Y.; Nakashima, N.; Asano, T. Electrostatic Inkjet Printing of Carbon Nanotube for Cold Cathode Application. *Jpn. J. Appl. Phys.* **2008**, *47*, 5109−5112.

(23) Small, W. R.; Panhuis, M. I. H. Inkjet Printing of Transparent, Electrically Conducting Single-Waited Carbon-Nanotube Composites. *Small* **2007**, *3*, 1500−1503.

(24) Song, J. W.; Kim, Y. S.; Yoon, Y. H.; Lee, E. S.; Han, C. S.; Cho, Y.; Kim, D.; Kim, J.; Lee, N.; Ko, Y. G.; et al. The Production of Transparent Carbon Nanotube Field Emitters Using Inkjet Printing. *Phys. E* **2009**, *41*, 1513−1516.

(25) Majumder, M.; Rendall, C.; Li, M.; Behabtu, N.; Eukel, J. A.; Hauge, R. H.; Schmidt, H. K.; Pasquali, M. Insights into the Physics of Spray Coating of Swnt Films. *Chem. Eng. Sci.* **2010**, *65*, 2000−2008.

(26) Dan, B.; Irvin, G. C.; Pasquali, M. Continuous and Scalable Fabrication of Transparent Conducting Carbon Nanotube Films. *ACS Nano* **2009**, *3*, 835−843.

(27) Duggal, R.; Hussain, F.; Pasquali, M. Self-Assembly of Single-Walled Carbon Nanotubes into a Sheet by Drop Drying. *Adv. Mater.* **2006**, *18*, 29−34.

(28) Russell, J. M.; Oh, S. J.; LaRue, I.; Zhou, O.; Samulski, E. T. Alignment of Nematic Liquid Crystals Using Carbon Nanotube Films. *Thin Solid Films* **2006**, *509*, 53−57.

(29) Shimoda, H.; Oh, S. J.; Geng, H. Z.; Walker, R. J.; Zhang, X. B.; McNeil, L. E.; Zhou, O. Self-Assembly of Carbon Nanotubes. *Adv. Mater.* **2002**, *14*, 899−901.

(30) Vigolo, B.; Penicaud, A.; Coulon, C.; Sauder, C.; Pailler, R.; Journet, C.; Bernier, P.; Poulin, P. Macroscopic Fibers and Ribbons of Oriented Carbon Nanotubes. *Science* **2000**, *290*, 1331−1334.

(31) Gong, X. Y.; Liu, J.; Baskaran, S.; Voise, R. D.; Young, J. S. Surfactant-Assisted Processing of Carbon Nanotube/Polymer Composites. *Chem. Mater.* **2000**, *12*, 1049−1052.

(32) Islam, M. F.; Rojas, E.; Bergey, D. M.; Johnson, A. T.; Yodh, A. G. High Weight Fraction Surfactant Solubilization of Single-Wall Carbon Nanotubes in Water. *Nano Lett.* **2003**, *3*, 269−273.

(33) Pint, C. L.; Xu, Y.-Q.; Moghazy, S.; Cherukuri, T.; Alvarez, N. T.; Haroz, E. H.; Mahzooni, S.; Doorn, S. K.; Kono, J.; Pasquali, M.; et al. Dry Contact Transfer Printing of Aligned Carbon Nanotube Patterns and Characterization of Their Optical Properties for Diameter Distribution and Alignment. *ACS Nano* **2010**, *4*, 1131−1145.

(34) Walters, D. A.; Ericson, L. M.; Casavant, M. J.; Liu, J.; Colbert, D. T.; Smith, K. A.; Smalley, R. E. Elastic Strain of Freely Suspended Single-Wall Carbon Nanotube Ropes. *Appl. Phys. Lett.* **1999**, *74*, 3803−3805.

(35) Park, J. G.; Smithyman, J.; Lin, C. Y.; Cooke, A.; Kismarahardja, A. W.; Li, S.; Liang, R.; Brooks, J. S.; Zhang, C.; Wang, B. Effects of Surfactants and Alignment on the Physical Properties of Single-Walled Carbon Nanotube Buckypaper. *J. Appl. Phys.* **2009**, *106*, 104310.

(36) Song, W. H.; Kinloch, I. A.; Windle, A. H. Nematic Liquid Crystallinity of Multiwall Carbon Nanotubes. *Science* **2003**, *302*, 1363−1363.

(37) Song, W. H.; Windle, A. H. Isotropic-Nematic Phase Transition of Dispersions of Multiwall Carbon Nanotubes. *Macromolecules* **2005**, *38*, 6181−6188.

(38) Song, W. H.; Windle, A. H. Size-Dependence and Elasticity of Liquid-Crystalline Multiwalled Carbon Nanotubes. *Adv. Mater.* **2008**, *20*, 3149–3154.

(39) Davis, V. A.; Parra-Vasquez, A. N. G.; Green, M. J.; Rai, P. K.; Behabtu, N.; Prieto, V.; Booker, R. D.; Schmidt, J.; Kesselman, E.; Zhou, W.; et al. True Solutions of Single-Walled Carbon Nanotubes for Assembly into Macroscopic Materials. *Nat. Nanotechnol.* **2009**, *4*, 830–834.

(40) Behabtu, N.; Lomeda, J. R.; Green, M. J.; Higginbotham, A. L.; Sinitskii, A.; Kosynkin, D. V.; Tsentalovich, D.; Parra-Vasquez, A. N. G.; Schmidt, J.; Kesselman, E.; et al. Spontaneous High-Concentration Dispersions and Liquid Crystals of Graphene. *Nat. Nanotechnol.* **2010**, *5*, 406–411.

(41) Hecht, D. S.; Heintz, A. M.; Lee, R.; Hu, L.; Moore, B.; Cucksey, C.; Risser, S. High Conductivity Transparent Carbon Nanotube Films Deposited from Superacid. *Nanotechnology* **2011**, *22*, 075201.

(42) Saha, A.; Ghosh, S.; Weisman, R. B.; Martí, A. A. Films of Bare Single-Walled Carbon Nanotubes from Superacids with Tailored Electronic and Photoluminescence Properties. *ACS Nano* **2012**, *6*, 5727–5734.

(43) Mirri, F.; Ma, A. W. K.; Hsu, T. T.; Behabtu, N.; Eichmann, S. L.; Young, C. C.; Tsentalovich, D. E.; Pasquali, M. High-Performance Carbon Nanotube Transparent Conductive Films by Scalable Dip Coating. *ACS Nano* **2012**, *6*, 9737–9744.

(44) Cooper, S. M.; Chuang, H. F.; Cinke, M.; Cruden, B. A.; Meyyappan, M. Gas Permeability of a Buckypaper Membrane. *Nano Lett.* **2003**, *3*, 189–192.

(45) Dumee, L. F.; Sears, K.; Schutz, J.; Finn, N.; Huynh, C.; Hawkins, S.; Duke, M.; Gray, S. Characterization and Evaluation of Carbon Nanotube Bucky-Paper Membranes for Direct Contact Membrane Distillation. *J. Membr. Sci.* **2010**, *351*, 36–43.

(46) Smajda, R.; Kukovecz, A.; Konya, Z.; Kiricsi, I. Structure and Gas Permeability of Multi-Wall Carbon Nanotube Buckypapers. *Carbon* **2007**, *45*, 1176–1184.

(47) Gruner, G. Carbon Nanotube Films for Transparent and Plastic Electronics. *J. Mater. Chem.* **2006**, *16*, 3533–3539.

(48) Zhang, D.; Ryu, K.; Liu, X.; Polikarpov, E.; Ly, J.; Tompson, M. E.; Zhou, C. Transparent, Conductive, and Flexible Carbon Nanotube Films and Their Application in Organic Light-Emitting Diodes. *Nano Lett.* **2006**, *6*, 1880–1886.

(49) Hecht, D. S.; Thomas, D.; Hu, L.; Ladous, C.; Lam, T.; Park, Y.; Irvin, G.; Drzaic, P. Carbon-Nanotube Film on Plastic as Transparent Electrode for Resistive Touch Screens. *J. Soc. Inf. Display* **2009**, *17*, 941–946.

(50) Davis, V. A.; Ericson, L. M.; Parra-Vasquez, A. N. G.; Fan, H.; Wang, Y. H.; Prieto, V.; Longoria, J. A.; Ramesh, S.; Saini, R. K.; Kittrell, C.; et al. Phase Behavior and Rheology of Swnts in Superacids. *Macromolecules* **2004**, *37*, 154–160.

(51) Rai, P. K.; Pinnick, R. A.; Parra-Vasquez, A. N. G.; Davis, V. A.; Schmidt, H. K.; Hauge, R. H.; Smalley, R. E.; Pasquali, M. Isotropic-Nematic Phase Transition of Single-Walled Carbon Nanotubes in Strong Acids. *J. Am. Chem. Soc.* **2006**, *128*, 591–595.

(52) Green, M. J.; Parra-Vasquez, A. N. G.; Behabtu, N.; Pasquali, M. Modeling the Phase Behavior of Polydisperse Rigid Rods with Attractive Interactions with Applications to Single-Walled Carbon Nanotubes in Superacids. *J. Chem. Phys.* **2009**, *131*, 084901.

(53) Davis, V. A. Liquid Crystalline Assembly of Nanocylinders. *J. Mater. Res.* **2011**, *26*, 140–153.

(54) Puech, N.; Grelet, E.; Poulin, P.; Blanc, C.; van der Schoot, P. Nematic Droplets in Aqueous Dispersions of Carbon Nanotubes. *Phys. Rev. E* **2010**, *82*, 020702.

(55) Donald, A. M.; Windle, A. H.; Hanna, S., *Liquid Crystalline Polymers*; Cambridge University Press: Cambridge, 2005.

(56) Spontak, R. J.; Windle, A. H. Electron Microscopy of Non-Periodic Layer Crystallites in Thermotropic Random Copolymers. *J. Mater. Sci.* **1990**, *25*, 2727–2736.

(57) Olley, R. H.; Hodge, A. M.; Bassett, D. C. Permanganic Etchant for Polyolefins. *J. Polym. Sci., Part B: Polym. Phys.* **1979**, *17*, 627–643.

(58) Olley, R. H.; Bassett, D. C. An Improved Permanganic Etchant for Polyolefines. *Polymer* **1982**, *23*, 1707–1710.

(59) Olley, R. H.; Bassett, D. C.; Blundell, D. J. Permanganic Etching of Peek. *Polymer* **1986**, *27*, 344–348.

(60) Henrard, L.; Loiseau, A.; Journet, C.; Bernier, P. Study of the Symmetry of Single-Wall Nanotubes by Electron Diffraction. *Eur. Phys. J. B* **2000**, *13*, 661–669.

(61) Rols, S.; Almairac, R.; Henrard, L.; Anglaret, E.; Sauvajol, J.-L. Diffraction by Finite-Size Crystalline Bundles of Single Wall Nanotubes. *Eur. Phys. J. B* **1999**, *10*, 263–270.

(62) Colomer, J. F.; Henrard, L.; Launois, P.; Van Tendeloo, G.; Lucas, A. A.; Lambin, P. Interpretation of Electron Diffraction from Carbon Nanotube Bundles Presenting Precise Helicity. *Phys. Rev. B* **2004**, *70*, 075408.

(63) Kistler, S. F.; Scriven, L. E. Coating Flow Theory by Finite Element and Asymptotic Analysis of the Navier-Stokes System. *Int. J. Numer. Methods Fluids* **1984**, *4*, 207–229.

(64) Nam, J.; Scriven, L. E.; Carvalho, M. S. Tracking Birth of Vortex in Flows. *J. Comput. Phys.* **2009**, *228*, 4549–4567.

(65) Papanastasiou, T. C.; Malamataris, N.; Ellwood, K. A New Outflow Boundary Condition. *Int. J. Numer. Methods Fluids* **1992**, *14*, 587–608.

(66) Larson, R. G. *The Structure and Rheology of Complex Fluids*; Oxford University Press: New York, Oxford, 1999.

(67) Duggal, R.; Pasquali, M. Dynamics of Individual Single-Walled Carbon Nanotubes in Water by Real-Time Visualization. *Phys. Rev. Lett.* **2006**, *96*.

(68) Parra-Vasquez, A. N. G.; Stepanek, I.; Davis, V. A.; Moore, V. C.; Haroz, E. H.; Shaver, J.; Hauge, R. H.; Smalley, R. E.; Pasquali, M. Simple Length Determination of Single-Walled Carbon Nanotubes by Viscosity Measurements in Dilute Suspensions. *Macromolecules* **2007**, *40*, 4043–4047.

(69) Fonck, E.; Feigl, G. G.; Fasel, J.; Sage, D.; Unser, M.; Rufenacht, D. A.; Stergiopulos, N. Effect of Aging on Elastin Functionality in Human Cerebral Arteries. *Stroke* **2009**, *40*, 2552–2556.

(70) Gutfinger, C.; Tallmadge, J. A. Films of Non-Newtonian Fluids Adhering to Flat Plates. *AIChE J.* **1965**, *11*, 403–413.

(71) Geng, H. Z.; Kim, K. K.; So, K. P.; Lee, Y. S.; Chang, Y.; Lee, Y. H. Effect of Acid Treatment on Carbon Nanotube-Based Flexible Transparent Conducting Films. *J. Am. Chem. Soc.* **2007**, *129*, 7758.

(72) Green, M. J.; Behabtu, N.; Pasquali, M.; Adams, W. W. Nanotubes as Polymers. *Polymer* **2009**, *50*, 4979–4997.

(73) Parra-Vasquez, A. N. G.; Behabtu, N.; Green, M. J.; Pint, C. L.; Young, C. C.; Schmidt, J.; Kesselman, E.; Goyal, A.; Ajayan, P. M.; Cohen, Y.; et al. Spontaneous Dissolution of Ultralong Single- and Multiwalled Carbon Nanotubes. *ACS Nano* **2010**, *4*, 3969–3978.

(74) Nikolaev, P.; Bronikowski, M. J.; Bradley, R. K.; Rohmund, F.; Colbert, D. T.; Smith, K. A.; Smalley, R. E. Gas-Phase Catalytic Growth of Single-Walled Carbon Nanotubes from Carbon Monoxide. *Chem. Phys. Lett.* **1999**, *313*, 91–97.